

## Structural Analysis of PdAu Dendrimer-Encapsulated Bimetallic Nanoparticles

Michael G. Weir,<sup>†</sup> Marc R. Knecht,<sup>†,§</sup> Anatoly I. Frenkel,<sup>\*,‡</sup> and Richard M. Crooks<sup>\*,†</sup><sup>†</sup>Department of Chemistry and Biochemistry, Texas Materials Institute, Center for Nano- and Molecular Science and Technology, The University of Texas at Austin, 1 University Station, A5300, Austin, Texas 78712-0165, and <sup>‡</sup>Department of Physics, Yeshiva University, 245 Lexington Ave., New York, New York 10016.<sup>§</sup>Current address: Department of Chemistry, University of Kentucky, 125 Chemistry-Physics Building, Lexington, KY 40506

Received June 21, 2009. Revised Manuscript Received August 19, 2009

PdAu dendrimer-encapsulated nanoparticles (DENs) were prepared via sequential reduction of the component metals. When Au is reduced onto 55-atom, preformed Pd DEN cores, analysis by UV-vis spectroscopy, electron microscopy, and extended X-ray absorption fine structure (EXAFS) spectroscopy leads to a model consistent with inversion of the two metals. That is, Au migrates into the core and Pd resides on the surface. However, when Pd is reduced onto a 55-atom Au core, the expected Au core-Pd shell structure results. In this latter case, the EXAFS analysis suggests partial oxidation of the relatively thick Pd shell. When the DENs are extracted from their protective dendrimer stabilizers by alkylthiols, the resulting monolayer-protected clusters retain their original Au core-Pd shell structures. The structural analysis is consistent with a study of nanoparticle-catalyzed conversion of resazurin to resorufin. The key conclusion from this work is that correlation of structure to catalytic function for very small, bimetallic nanoparticles requires detailed information about atomic configuration.

## Introduction

Here we report the synthesis and characterization of bimetallic PdAu dendrimer-encapsulated nanoparticles (DENs) prepared via sequential reduction of the component metals in hydroxyl-terminated poly(amidoamine) (PAMAM) dendrimers (Scheme 1).<sup>1</sup> We have previously reported that this approach can be used to prepare nanoparticles comprised of a core of the first metal covered with a shell of the second metal.<sup>2,3</sup> The key result to emerge from the present study is that regardless of whether Pd or Au is reduced first, these DENs adopt a Au core-Pd shell (Au@Pd) structure. Primary evidence for this contention comes from detailed measurements made by extended X-ray absorption fine structure (EXAFS) spectroscopy. Additionally, the Au-catalyzed conversion of resazurin to resorufin is used to probe the surface composition of the DENs, and the results are consistent with the EXAFS data.<sup>4</sup> Finally, we also show that Au@Pd DENs can be extracted from within their host dendrimers with their core-shell structures intact by using appropriate  $\alpha$ -alkylthiol ligands.

DENs are usually synthesized in a two-step process. First, metal ions are extracted from solution into the dendrimer interior via complexation with internal tertiary amines. Second, the metal ions are reduced with  $\text{BH}_4^-$ , and the resultant atoms subsequently coalesce to form zerovalent nanoparticles within the dendrimer templates. Monometallic Au, Pt, Pd, Cu, Ni, Ru, Rh, Ir, and Fe,

as well as bimetallic AuAg, PdAu, PdPt, PtCu, PtAu, and CuPd DENs, have been synthesized using this basic procedure.<sup>1-3,5-22</sup> Once formed, DENs are retained within and stabilized by the dendrimer framework.<sup>1</sup>

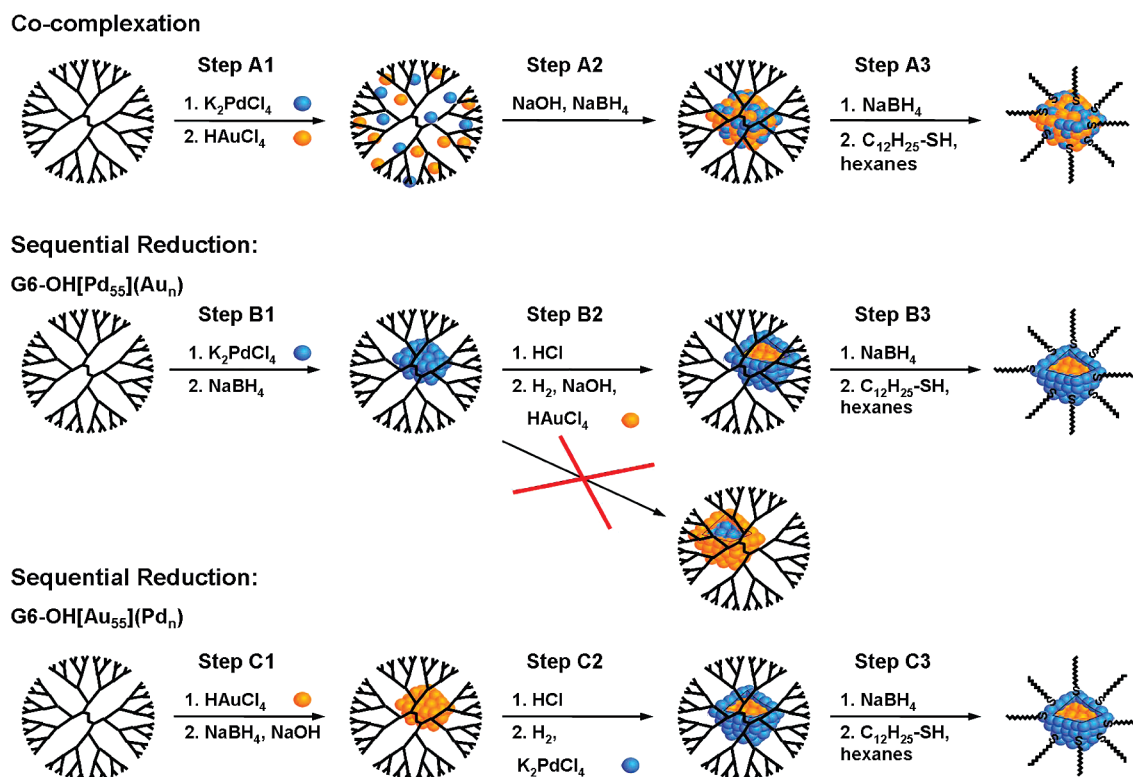
We have previously reported the synthesis of PdAu bimetallic nanoparticles using two different methods: co-complexation of both precursor metal ions followed by simultaneous reduction<sup>2,7,23</sup> and sequential complexation and reduction of each of the two metals (Scheme 1).<sup>2</sup> The first report of PdAu DENs

(6) Hoover, N. N.; Auten, B. J.; Chandler, B. D. *J. Phys. Chem. B* **2006**, *110*, 8606-8612.(7) Knecht, M. R.; Weir, M. G.; Frenkel, A. I.; Crooks, R. M. *Chem. Mater.* **2008**, *20*, 1019-1028.(8) Lang, H.; Maldonado, S.; Stevenson, K. J.; Chandler, B. D. *J. Am. Chem. Soc.* **2004**, *126*, 12949-12956.(9) Knecht, M. R.; Garcia-Martinez, J. C.; Crooks, R. M. *Chem. Mater.* **2006**, *18*, 5039-5044.(10) Knecht, M. R.; Garcia-Martinez, J. C.; Crooks, R. M. *Langmuir* **2005**, *21*, 11981-11986.(11) Beakley, L. W.; Yost, S. E.; Cheng, R.; Chandler, B. D. *Appl. Catal., A* **2005**, *292*, 124-129.(12) Bustos, E. B.; Jimenez, M. G. G.; Diaz-Sanchez, B. R.; Juaristi, E.; Chapman, T. W.; Godinez, L. A. *Talanta* **2007**, *72*, 1586-1592.(13) Chung, Y.-M.; Rhee, H.-K. *Catal. Lett.* **2003**, *85*, 159-164.(14) Gilbertson, J. D.; Vijayaraghavan, G.; Stevenson, K. J.; Chandler, B. D. *Langmuir* **2007**, *23*, 11239-11245.(15) Hendricks, T. R.; Dams, E. E.; Wensing, S. T.; Lee, I. *Langmuir* **2007**, *23*, 7404-7410.(16) Knecht, M. R.; Crooks, R. M. *New J. Chem.* **2007**, *31*, 1349-1353.(17) Lafaye, G.; Siani, A.; Marecot, P.; Amiridis, M. D.; Williams, C. T. *J. Phys. Chem. B* **2006**, *110*, 7725-7731.(18) Mark, S. S.; Bergkvist, M.; Yang, X.; Angert, E. R.; Batt, C. A. *Biomacromolecules* **2006**, *7*, 1884-1897.(19) Pittelkow, M.; Brock-Nannestad, T.; Moth-Poulsen, K.; Christensen, J. B. *Chem. Commun.* **2008**, 2358-2360.(20) Satoh, N.; Nakashima, T.; Kamikura, K.; Yamamoto, K. *Nat. Nanotechnol.* **2008**, *3*, 106-111.(21) Huang, W.; Kuhn, J. N.; Tsung, C.-K.; Zhang, Y.; Habas, S. E.; Yang, P.; Somorjai, G. A. *Nano Lett.* **2008**, *8*, 2027-2034.(22) Ye, H.; Crooks, R. M. *J. Am. Chem. Soc.* **2007**, *129*, 3627-3633.(23) Scott, R. W. J.; Sivadinarayana, C.; Wilson, O. M.; Yan, Z.; Goodman, D. W.; Crooks, R. M. *J. Am. Chem. Soc.* **2005**, *127*, 1380-1381.

\*To whom correspondence should be addressed: e-mail anatoly.frenkel@yu.edu, Ph 212-340-7827 (A.I.F.); e-mail crooks@cm.utexas.edu, Ph 512-475-8674 (R.M.C.).

(1) Scott, R. W. J.; Wilson, O. M.; Crooks, R. M. *J. Phys. Chem. B* **2005**, *109*, 692-704.(2) Scott, R. W. J.; Wilson, O. M.; Oh, S. K.; Kenik, E. A.; Crooks, R. M. *J. Am. Chem. Soc.* **2004**, *126*, 15583-15591.(3) Wilson, O. M.; Scott, R. W. J.; Garcia-Martinez, J. C.; Crooks, R. M. *J. Am. Chem. Soc.* **2005**, *127*, 1015-1024.(4) Xu, W.; Kong, J. S.; Yeh, Y.-T. E.; Chen, P. *Nat. Mater.* **2008**, *7*, 992-996.(5) Endo, T.; Yoshimura, T.; Esumi, K. *J. Colloid Interface Sci.* **2005**, *286*, 602-609.

Scheme 1



described the products of both the co-complexation and sequential methods using both partially quaternized, amine-terminated dendrimers and hydroxyl-terminated dendrimers.<sup>2</sup> UV-vis spectroscopy and selective catalysis experiments indirectly confirmed structural differences between DENs prepared by co-complexation and sequential reduction. We also suggested, on the basis of fairly weak evidence, that there might be differences in the structures of core-shell PdAu DENs depending on which metal was used as the seed (core). In the present paper, using more sophisticated analysis tools, we recognize that regardless of whether Au or Pd is used as the initial seed, the product of the sequential reduction is a Au@Pd DEN.

In addition to the detailed study described in the previous paragraph, we also reported that PdAu alloy DENs prepared within primary amine-terminated PAMAM dendrimers via the co-complexation route could be immobilized on titania substrates.<sup>23</sup> However, this report focused on the catalytic oxidation of CO, and little structural analysis was presented. Finally, we very recently reported a detailed EXAFS analysis of PdAu bimetallic DENs synthesized via co-complexation within sixth-generation, hydroxyl-terminated (G6-OH) PAMAM dendrimers.<sup>7</sup> Consistent with our preliminary report,<sup>2</sup> these results showed that PdAu DENs prepared by co-complexation form alloys. However, we described these DENs as quasi-random alloys because they were somewhat enriched with Pd on their surface and with Au within their interior. We also showed that these PdAu alloys could be converted into Au@Pd monolayer-protected clusters (MPCs)<sup>24,25</sup> via intradendrimer dealloying and subsequent reduction.

Chandler and co-workers have prepared PtCu,<sup>6</sup> PtAu,<sup>8</sup> and NiAu<sup>26</sup> nanoparticles via dendrimer templating. The PtCu DENs were synthesized by co-complexation while preparation of the PtAu DENs involved galvanic exchange. The NiAu nanoparticles were stabilized by multiple dendrimers rather than being encapsulated within single dendrimers.<sup>26,27</sup> The surface composition of supported PtCu DENs was inferred from catalytic measurements of toluene hydrogenation and CO oxidation. Specifically, Pt dominated the catalytic properties in the presence of CO, while Cu had a strong negative influence on the catalytic rate during hydrogenation. The data were interpreted in terms of structural rearrangements driven by CO.

There have been numerous reports from other groups concerning the synthesis of PdAu bimetallic nanoparticles prepared by means other than dendrimer templating.<sup>28,29</sup> However, here we focus only on unsupported PdAu particles having diameters of  $< \sim 5$  nm, as they are most closely related to the DENs discussed in this paper. Different synthetic methods are capable of producing nanoparticles with alloy,<sup>30,31</sup> core-shell,<sup>29,32–34</sup> and other more complex structures.<sup>35,36</sup> The structures of PdAu alloys range from truly random<sup>30</sup> to partially segregated, quasi-random alloys.<sup>7,31</sup> In this small size range, most core-shell particles formed are Au@Pd,<sup>29</sup> but larger particles may form the opposite

(24) Murray, R. W. *Chem. Rev.* **2008**, *108*, 2688–2720.

(25) Templeton, A. C.; Wuelfing, W. P.; Murray, R. W. *Acc. Chem. Res.* **2000**, *33*, 27–36.

(26) Auten, B. J.; Hahn, B. P.; Vijayaraghavan, G.; Stevenson, K. J.; Chandler, B. D. *J. Phys. Chem. C* **2008**, *112*, 5365–5372.

(27) Garcia, M. E.; Baker, L. A.; Crooks, R. M. *Anal. Chem.* **1999**, *71*, 256–258.

(28) Ferrando, R.; Jellinek, J.; Johnston, R. L. *Chem. Rev.* **2008**, *108*, 845–910.

(29) Mandal, S.; Mandale, A. B.; Sastry, M. *J. Mater. Chem.* **2004**, *14*.

(30) Perez-Tijerina, E.; Pinilla, M. G.; Mejia-Rosales, S.; Ortiz-Mendez, U.; Torres, A.; Jose-Yacamán, M. *Faraday Discuss.* **2008**, *138*, 353–362.

(31) Wu, M. L.; Chen, D. H.; Huang, T. C. *Langmuir* **2001**, *17*, 3877–3883.

(32) Harpeness, R.; Gedanken, A. *Langmuir* **2004**, *20*, 3431–3434.

(33) Jose, D.; Jagirdar, B. R. *J. Phys. Chem. C* **2008**, *112*, 10089–10094.

(34) Kan, C.; Cai, W.; Li, C.; Zhang, L.; Hofmeister, H. *J. Phys. D: Appl. Phys.* **2003**, *36*, 1609–1614.

(35) Ferrer, D.; Blom, D. A.; Allard, L. F.; Mejia, S.; Perez-Tijerina, E.; Jose-Yacamán, M. *J. Mater. Chem.* **2008**, *18*, 2442–2446.

(36) Mejia-Rosales, S. J.; Fernandez-Navarro, C.; Perez-Tijerina, E.; Blom, D. A.; Allard, L. F.; Jose-Yacamán, M. *J. Phys. Chem. C* **2007**, *111*, 1256–1260.

structure.<sup>34</sup> Jose-Yacaman and co-workers have used aberration-corrected TEM to demonstrate a three-layer structure that varies as a function of the diameter of the particle and the ratio of the two metals.<sup>35,36</sup> They have also used inert-gas condensation in a sputter reactor to synthesize alloyed PdAu bimetallic nanoparticles.<sup>30</sup> Classical molecular dynamics simulations have shown that the Pd@Au structure is the most stable form thermodynamically,<sup>37</sup> but these calculations do not include ligand effects or other conditions present during a real synthesis.

X-ray absorption spectroscopy (XAS) is a powerful tool for determining the structure of bimetallic nanoparticles.<sup>38–40</sup> For example, a case that is particularly relevant to that discussed here was carried out by Toshima and co-workers. They investigated polymer-protected PdAu clusters prepared by both simultaneous<sup>41</sup> and sequential<sup>42</sup> reduction. A Au@Pd structure was determined for the simultaneous reduction case. The sequential reduction process yielded two different results, depending on the order of reduction of the metals. When Pd was reduced first, bimetallic cluster-in-cluster structures were observed.<sup>42</sup> When Au was reduced first, a mixture of Pd and Au monometallic nanoparticles was formed. XAS studies have been carried out on other larger PdAu nanoparticles in solution<sup>43</sup> and on supported PdAu clusters.<sup>44–46</sup>

Here we used UV–vis spectroscopy, TEM, EXAFS, and a Au-specific catalytic reaction to elucidate the structure of bimetallic PdAu DENs prepared within G6-OH dendrimers via the sequential reduction method illustrated in Scheme 1. Specifically, Au and Pd seed DENs were prepared, and then the second metal was catalytically reduced onto the seeds. UV–vis spectroscopy confirms that the precursor metal ions are complexed and then reduced. TEM size-distribution analysis shows that the sizes of these particles are consistent with expectations based on their composition and the average number of atoms per particle. EXAFS reveals that a Au@Pd structure forms in DENs prepared by sequential reduction regardless of the order that the component metals are introduced. When extracted from the dendrimer interior with dodecanethiol, the particles retain their Au@Pd structure but with an unanticipated degree of Pd–S bonding. A comprehensive study of the catalytic conversion of resazurin to resorufin indicates that monometallic Au DENs are highly active. However, bimetallic DENs having Pd-only shells, or even shells composed of both Pd and Au, are not active. This suggests that particular arrangements of Au atoms on the nanoparticle surface are required for catalytic activity.

## Experimental Section

**Chemicals.** G6-OH PAMAM dendrimers were purchased from Dendritech, Inc. (Midland, MI), as methanol solutions. Prior to use, the dendrimer stock solution was dried under vacuum and then redissolved in sufficient deionized water to make a 100  $\mu\text{M}$  solution. All other chemicals were used as received

unless otherwise noted in the text. Resazurin,  $\text{K}_2\text{PdCl}_4$ ,  $\text{NaBH}_4$ ,  $\text{HAuCl}_4 \cdot 3\text{H}_2\text{O}$ , and dodecanethiol were purchased from Sigma-Aldrich (Milwaukee, WI), and NaOH, HCl, and hexanes were purchased from Fisher Scientific (Pittsburgh, PA). Absolute ethanol was purchased from Aaper Chemical Co. (Shelbyville, KY). Aqueous solutions were prepared using 18  $\text{M}\Omega \cdot \text{cm}$  Milli-Q water (Millipore, Bedford, MA).

**Characterization.** UV–vis absorbance spectra were obtained using a Hewlett-Packard HP8453 spectrometer and quartz cuvettes having an optical path length of 0.200 cm. Depending on the sample, a spectrum of either 2.00  $\mu\text{M}$  G6-OH in water or neat hexanes (no dendrimer) was used for background subtraction. TEM micrographs were obtained using a JEOL-2010F TEM operating at 200 kV. Samples were prepared by dropwise addition of an appropriate solution onto a 20 nm thick, carbon-coated, 400 mesh Cu grid (EM Sciences, Gibbstown, NJ) followed by solvent evaporation in air.

EXAFS experiments were conducted at beamline X18B of the National Synchrotron Light Source at the Brookhaven National Laboratory. The DEN solutions were freeze-dried using a Labconco FreeZone 12 L lyophilizer to simplify transporting them to the beamline. Subsequently, the powder was partially reconstituted in methanol or hexanes for dispersion onto adhesive tape, followed by drying in air. The tapes were folded multiple times to ensure homogeneity. The samples were measured in fluorescence mode, using an Ar-filled, five-grid Lytle detector, with the sample positioned at a 45° angle relative to the incident beam. X-ray absorption coefficients were measured from 150 eV below to 750 and 1250 eV above the Pd K and Au L<sub>3</sub> edges, respectively. The X-ray energy was calibrated prior to examination of each metallic edge by analysis of the corresponding bulk metal foil. EXAFS data were analyzed using the IFEFFIT software package.<sup>47</sup>

**Synthesis of the Monometallic Seed DENs.** The synthesis of both Pd and Au monometallic DENs has previously been described.<sup>1,48,49</sup> However, the EXAFS studies required larger quantities of DENs, so the synthesis was scaled up in the present case. Briefly, 5.0 mL of a 100.0  $\mu\text{M}$  G6-OH stock solution was diluted with enough water (~240 mL) to yield a final concentration of 2.00  $\mu\text{M}$ . For G6-OH(Pd<sub>55</sub>) DENs, 55 equiv of a freshly prepared 10.0 mM  $\text{K}_2\text{PdCl}_4$  solution (2.75 mL) was added to the G6-OH solution. The solution was allowed to stir for a minimum of 15 min to ensure complete complexation between the tertiary amines of the dendrimer and  $\text{Pd}^{2+}$ . We denote all forms of ionic Pd as  $\text{Pd}^{2+}$  for convenience and all forms of ionic Au as  $\text{Au}^{3+}$ , even though various hydrolysis products of  $\text{PdCl}_4^{2-}$  likely exist.<sup>50,51</sup> Next, a 10-fold molar excess of an aqueous 1.00 M  $\text{NaBH}_4$  solution was added to the dendrimer/metal ion precursor. Reduction was allowed to proceed for 15 min. The final volume of each solution was 250 mL.

For the G6-OH(Au<sub>55</sub>) DENs, a similar procedure was followed. After dilution of the dendrimer stock, 55 equiv of a 10.0 mM  $\text{HAuCl}_4$  solution (2.75 mL) was added to the G6-OH solution. This was followed almost immediately (< 1 min) by addition of a 10-fold molar excess of 1.00 M  $\text{NaBH}_4$  in 0.30 M aqueous NaOH (0.27 mL). Quick addition of  $\text{NaBH}_4$  and the presence of base are necessary to prevent reduction of the Au salt to zerovalent metal by the hydroxyl functionalities of the dendrimer.<sup>52</sup>

**Synthesis of the Shell.** Sequentially reduced DENs having a nominal 55-atom Pd core and either 92 or 254 Au atoms in the

(37) Liu, H. B.; Pal, U.; Perez, R.; Ascencio, J. A. *J. Phys. Chem. B* **2006**, *110*, 5191–5195.

(38) Frenkel, A. I. *Z. Kristallogr.* **2007**, *222*, 605–611.

(39) Glasner, D.; Frenkel, A. I. *XAFS 13, Proc. Int. Conf. X-ray Absorpt. Fine Struct.* **2007**, *882*, 746–748.

(40) Hwang, B. J.; Sarma, L. S.; Chen, J.-M.; Chen, C. H.; Shih, S.-C.; Wang, G. R.; Liu, D. G.; Lee, J. F.; Tang, M. T. *J. Am. Chem. Soc.* **2005**, *127*, 11140–11145.

(41) Toshima, N.; Harada, M.; Yamazaki, Y.; Asakura, K. *J. Phys. Chem.* **1992**, *96*, 9927–9933.

(42) Harada, M.; Asakura, K.; Toshima, N. *J. Phys. Chem.* **1993**, *97*, 5103–5114.

(43) Chen, C.-H.; Sarma, L. S.; Chen, J.-M.; Shih, S.-C.; Wang, G.-R.; Liu, D.-G.; Tang, M.-T.; Lee, J.-F.; Hwang, B.-J. *ACS Nano* **2007**, *1*, 114–125.

(44) Davis, R. J.; Boudart, M. *J. Phys. Chem.* **1994**, *98*, 5471–5477.

(45) Reifsnnyder, S. N.; Lamb, H. H. *J. Phys. Chem. B* **1999**, *103*, 321–329.

(46) Zhang, P.; Zhou, X.; Tang, Y.; Sham, T. K. *Langmuir* **2005**, *21*, 8502–8508.

(47) Newville, M. *J. Synchrotron Radiat.* **2001**, *8*, 322–324.

(48) Kim, Y. G.; Oh, S. K.; Crooks, R. M. *Chem. Mater.* **2004**, *16*, 167–172.

(49) Scott, R. W. J.; Ye, H.; Henriquez, R. R.; Crooks, R. M. *Chem. Mater.* **2003**, *15*, 3873–3878.

(50) Kim, Y. H.; Nakano, Y. *Water Res.* **2005**, *39*, 1324.

(51) Tait, C. D.; Janecky, D. R.; Rogers, P. S. Z. *Geochim. Cosmochim. Acta* **1991**, *55*, 1253–1264.

(52) Garcia-Martinez, J. C.; Crooks, R. M. *J. Am. Chem. Soc.* **2004**, *126*, 16170–16178.

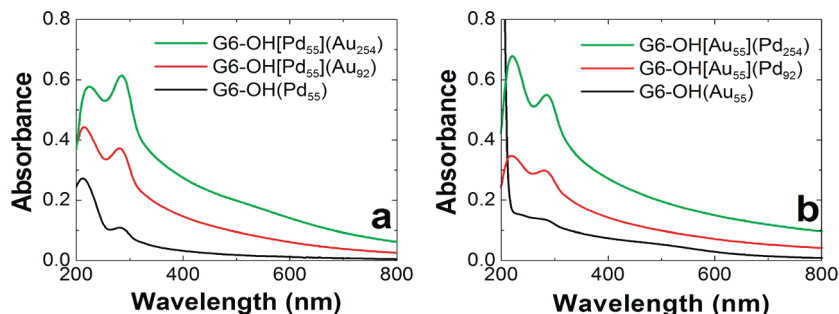


**Figure 1.** UV-vis spectra of (a) Pd monometallic DENs and PdAu DENs formed by sequential reduction of Au onto a Pd core and (b) Au monometallic DENs and PdAu DENs formed by sequential reduction of Pd onto a Au core. The concentration of the DENs solutions was  $2.00 \mu\text{M}$ , and the analysis was carried out in a  $0.20 \text{ cm}$  cuvette.

putative shell were prepared as follows. 10 min after formation of the monometallic Pd DEN core,  $1.50 \text{ mL}$  of  $0.30 \text{ M HCl}$  was added to the solution to quench unreacted reducing equivalents of  $\text{BH}_4^-$ . A few minutes later,  $\text{H}_2$  gas was bubbled through the solution. After  $\sim 10 \text{ min}$ ,  $2.25 \text{ mL}$  of  $0.30 \text{ M NaOH}$  was added to neutralize the acid and ensure a basic pH (to slow reduction of the Au salt by hydroxyl groups of the dendrimer). Next, 92 or 254 equiv of  $10.0 \text{ mM HAuCl}_4$  solution was added ( $4.60$  and  $12.7 \text{ mL}$ , respectively). Bubbling of  $\text{H}_2$  gas was continued for an additional 15 min.

Sequentially reduced DENs having a nominal 55-atom Au core and either 92 or 254 Pd atoms in the putative shell were prepared as follows. A 10% molar excess (with respect to the NaOH present in solution) of  $0.30 \text{ M HCl}$  ( $0.30 \text{ mL}$ ) was added to the monometallic Au core DENs.  $\text{H}_2$  gas was then bubbled through the solution for a minimum of 10 min. While bubbling, either 92 or 254 equiv ( $4.60$  and  $12.7 \text{ mL}$ , respectively) of a fresh  $10.0 \text{ mM K}_2\text{PdCl}_4$  solution was added. Bubbling of  $\text{H}_2$  gas was continued for an additional 15 min.

**Extraction of DENs.** Extraction of the bimetallic PdAu DENs was carried out within 4 h of the initial reduction using a previously described method.<sup>52–55</sup> The solutions were exposed to air during this period and during the extraction process, resulting in partial oxidation of the zerovalent Pd within the DENs.<sup>56</sup> Briefly,  $125 \text{ mL}$  of an aqueous  $2.00 \mu\text{M}$  DEN solution was placed into a separatory funnel. A 100-fold excess (with respect to the total metal concentration) of solid  $\text{NaBH}_4$  was added. Next,  $125 \text{ mL}$  of a  $29.4 \text{ mM}$  dodecanethiol solution, prepared in hexanes, was layered atop the aqueous solution. The separatory funnel was shaken vertically and vigorously for 5 min. After settling, the organic phase was removed and collected. This process was repeated a total of six times: once for each of six  $125 \text{ mL}$  aliquots. At the end, all six extraction volumes ( $750 \text{ mL}$ ) were combined and then concentrated on a rotary evaporator to a volume of  $\sim 5.0 \text{ mL}$ . The resulting MPCs were then precipitated with absolute ethanol to separate them from excess dodecanethiol,<sup>52,55</sup> and the precipitate was collected by centrifugation. The supernatant was decanted, and the MPCs were redissolved in a small volume of hexanes. The concentrated solution was then evaporated to dryness under vacuum at  $23 \pm 2 \text{ }^\circ\text{C}$ .

**Resazurin Catalysis.**  $200.0 \mu\text{L}$  of each DEN sample ( $2.00 \mu\text{M}$  in dendrimer) was added to  $10.0 \text{ mL}$  of a  $10.0 \mu\text{M}$  aqueous resazurin solution. Solutions were stirred for 5 min before UV-vis spectra were obtained. In some cases, an additional spectrum was obtained 24 h later to ensure completion of the reaction.

## Results and Discussion

**Nomenclature.** We use  $\text{Au}_x\text{Pd}_y$  to represent particles formed by co-complexation. For sequentially reduced DENs, the notation  $\text{G6-OH}[\text{Au}_x](\text{Pd}_y)$  is used when Au is reduced first and Pd second, but this does not imply a particular alloy or core-shell structure. Likewise,  $\text{G6-OH}[\text{Pd}_x](\text{Au}_y)$  represents the case when Pd is reduced first and Au second. The numbers  $x$  and  $y$  represent the stoichiometric relationship of the metal-ion-to-dendrimer ratios used in the synthesis (that is, the average number of Au and Pd atoms in the DENs). We have previously shown that the average numbers of each element in bimetallic DENs closely correspond to the actual stoichiometry of individual particles.<sup>22</sup> The notations  $\text{Pd@Au}$  and  $\text{Au@Pd}$  specifically imply core-shell structures with the first element corresponding to the core and the second to the shell metal.

**Synthesis of PdAu DENs.** Three methods for synthesizing bimetallic DENs are illustrated in Scheme 1. The co-complexation method (steps A1 and A2) generally leads to alloy formation.<sup>7</sup> The two sequential reduction methods can lead to core-shell or alloy DENs. For sequential reduction, the seed DENs are synthesized (steps B1 and C1) using the same methods we have previously used for monometallic DENs.<sup>1,49,52</sup> The second metal salt is added in the presence of a weaker reducing agent,  $\text{H}_2$  gas in this case, so that the ions are catalytically reduced only on the existing DEN seed (steps B2 and C2). The presence of  $\text{H}_2$  ensures that a galvanic exchange mechanism (displacement of Pd by  $\text{AuCl}_4^-$ , for example) is not operative.<sup>57</sup>

Figure 1 provides UV-vis spectroscopic data for the sequential synthesis of PdAu DENs. The spectra in Figure 1a are consistent with 55-atom Pd DENs and subsequent addition of sufficient Au to yield one and two shells (92 and 254 equiv of Au, respectively). In each case, a monotonically increasing absorbance toward lower wavelengths is observed. This is consistent with expectations from Mie theory for particles in this size range.<sup>58–61</sup> The spectra exhibit three features in the 200–300 nm range that merit comment. The absorbance of the dendrimer itself at  $\sim 200 \text{ nm}$  is very strong, resulting in inconsistencies in background subtraction. There is a ligand-to-metal charge transfer (LMCT) peak at  $220 \text{ nm}$  corresponding to slight ( $< 10\%$ ) oxidation of the  $\text{Pd}_{55}$  DENs and subsequent recomplexation of the ions to the dendrimer.<sup>49,56</sup> The peak at  $\sim 280 \text{ nm}$  may be related to a small amount of a catalytic decomposition product of the dendrimer<sup>49</sup> but more likely arises from specific and reversible intradendrimer

(53) Kim, Y. G.; Garcia-Martinez, J. C.; Crooks, R. M. *Langmuir* **2005**, *21*, 5485–5491.

(54) Wilson, O. M.; Scott, R. W. J.; Garcia-Martinez, J. C.; Crooks, R. M. *Chem. Mater.* **2004**, *16*, 4202–4204.

(55) Garcia-Martinez, J. C.; Scott, R. W. J.; Crooks, R. M. *J. Am. Chem. Soc.* **2003**, *125*, 11190–11191.

(56) Carino, E. V.; Knecht, M. R.; Crooks, R. M. *Langmuir* **2009**, *25*, 10279–10284.

(57) Zhao, M.; Crooks, R. M. *Chem. Mater.* **1999**, *11*, 3379–3385.

(58) Alvarez, M. M.; Khoury, J. T.; Schaaff, T. G.; Shafiqullin, M. N.; Vezmar, I.; Whetten, R. L. *J. Phys. Chem. B* **1997**, *101*, 3706–3712.

(59) Daniel, M. C.; Astruc, D. *Chem. Rev.* **2004**, *104*, 293–346.

(60) Roldughin, V. I. *Russ. Chem. Rev. (Engl. Transl.)* **2000**, *69*, 821–843.

(61) Link, S.; El-Sayed, M. A. *Int. Rev. Phys. Chem.* **2000**, *19*, 409–453.

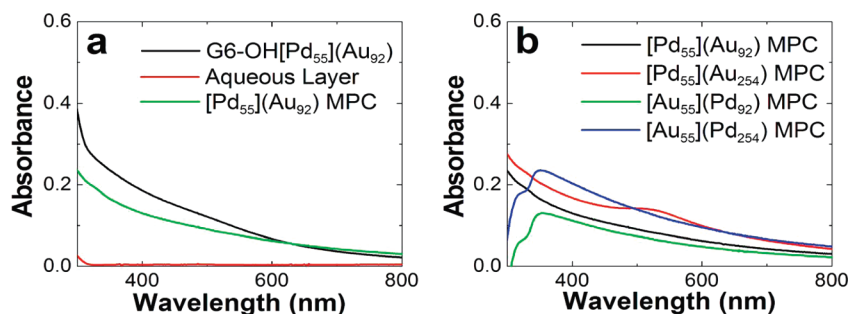


**Figure 2.** UV-vis spectra of PdAu DENs and MPCs prepared by extraction into hexanes using dodecanethiol as the phase transfer agent. (a) Spectra of an aqueous 2.00  $\mu\text{M}$  G6-OH[Pd<sub>55</sub>](Au<sub>92</sub>) DEN solution prior to extraction and the aqueous and hexane fractions after extraction. (b) Spectra for each MPC combination described in the text. These spectra are cut off below 300 nm because of the high absorbance of hexanes in this region. The path length of the cuvette was 0.20 cm.

configurational changes driven by pH.<sup>62</sup> Whatever the origin of this band, it does not appear to significantly affect the synthesis or catalytic properties of DENs. The increase in absorbance for the two types of PdAu particles, compared to the Pd-only DENs, is consistent with, but does not confirm, an increase in the size of the particles upon addition of Au.<sup>58–61</sup> A very slight plasmon band is centered at 522 nm for the G6-OH[Pd<sub>55</sub>](Au<sub>254</sub>) DENs.<sup>58–60,63,64</sup> The magnitude and position of this band are an indication that a very small fraction of these DENs have diameters in the 2–3 nm size range.<sup>65–68</sup>

The black spectrum in Figure 1b is consistent with 55-atom Au DENs,<sup>3,48,52</sup> and the other two spectra suggest further addition of Pd. The features of these spectra are similar to those in Figure 1a, except that the very small plasmon band, present at 505 nm for the Au<sub>55</sub> seed DENs, is absent. Additionally, the Pd<sup>2+</sup>-dendrimer LMCT band for the two bimetallics is slightly more pronounced. Finally, the similarity in the magnitudes of the absorbances of the spectra in Figure 1a,b suggests that regardless of the starting core metal, the particles have similar sizes and optical characteristics.

**Extraction of PdAu DENs.** Extraction of DENs from within dendrimer templates followed a previously established procedure that is briefly discussed in the Experimental Section.<sup>52,55</sup> The extraction model we have previously proposed involves two steps. First, a suitable ligand, typically an alkylthiol, is added to a solution of DENs. The ligand penetrates the dendrimer periphery and adsorbs to the surface of the encapsulated nanoparticle. Second, the presence of the ligand weakens the interaction between the nanoparticle and the dendrimer. If the ligand/DEN interaction is sufficiently strong, then binding results in extraction of the DEN into an organic phase. The empty dendrimer remains in the aqueous phase.

The spectra in Figure 2 provide evidence for extraction of the bimetallic DENs into hexanes using dodecanethiol as the phase-transfer agent. Figure 2a shows spectra of the precursor G6-OH[Pd<sub>55</sub>](Au<sub>92</sub>) DENs as well as both the aqueous and organic layers after extraction. The absorbance in the aqueous phase after extraction is negligible, indicating the absence of a detectable level of DENs. The spectrum of the organic layer is similar to that of the original DEN solution, indicating transfer of the metal nanoparticles to the organic phase. The small but

significant changes in the magnitudes of the absorbances may be related to differences in the ligands surrounding the nanoparticles (G6-OH vs dodecanethiol) or the dielectric constants of water and hexanes.<sup>58,61</sup>

Figure 2b shows spectra for all four compositions of the extracted, bimetallic MPCs. The monotonically increasing absorbances at lower wavelengths are in accordance with expectations for metal particles in this size range.<sup>1,65–68</sup> A broad plasmon is observed for the [Pd<sub>55</sub>](Au<sub>254</sub>) MPCs, similar to that found previously for Au and AuAg alloy MPCs having the same size.<sup>25</sup> The shoulder at  $\sim 340$  nm, and other differences in the spectra of the [Pd<sub>55</sub>](Au<sub>x</sub>) and [Au<sub>55</sub>](Pd<sub>x</sub>) MPCs near 300 nm, are a consequence of imperfect background subtraction (the solvent absorbs in this region). The important point is that MPCs having the same nominal size yield about the same absorbance at wavelengths  $> \sim 350$  nm.

**Size Analysis by TEM.** The size of the nanoparticles was determined by TEM. The diameters of the 55-atom Au and Pd seed DENs were both found to be  $1.2 \pm 0.3$  nm (Supporting Information, Figure S1).<sup>1,48,49,52,53,55</sup> This value is the same as for a 55-atom truncated cuboctahedron of these two metals.<sup>48</sup> When the second metal is added to the seeds, the particles become larger (Supporting Information, Figure S2). The bimetallic nanoparticles formed by sequential reduction are slightly larger than the corresponding monometallic nanoparticles composed of the same number of metal atoms. For example, 147-atom Au and Pd DENs have previously been found to be 1.6 nm in diameter (calculated: 1.6 nm), while here the bimetallics average  $2.0 \pm 0.5$  nm.<sup>1,48,49</sup> This increase may result from the presence of more atomic disorder in the bimetallics, but in any event the results are consistent with previous results obtained for DENs prepared by the sequential reduction method.<sup>2</sup>

Micrographs and histograms for the extracted MPCs are provided in the Supporting Information (Figure S3). The extracted, bimetallic MPCs are somewhat larger (0.2–0.3 nm) than the corresponding DENs. No such increase in size was evident in previous extraction experiments,<sup>7,52,55</sup> but in the present case it may be attributable to the incorporation of sulfur atoms from the alkylthiol into the Pd crystal structure. This type of configuration has been observed previously for other types of thiol-stabilized Pd nanoparticles and is discussed in more detail later.<sup>69</sup>

**Structural Analysis by EXAFS.** EXAFS was used to determine the average local structure of the DENs and MPCs. In this analysis, the coordination numbers (CNs) for each sample are compared to those calculated for different structural models. For

(62) Pande, S.; Crooks, R. M. 2009, manuscript in preparation.

(63) Mulvaney, P. *Langmuir* **1996**, *12*, 788–800.

(64) Zheng, J.; Petty, J. T.; Dickson, R. M. *J. Am. Chem. Soc.* **2003**, *125*, 7780–7781.

(65) Bauer, C.; Abid, J.-P.; Girault, H. H. *Chem. Phys.* **2005**, *319*, 409–421.

(66) Lim, I. S.; Pan, Y.; Mott, D.; Ouyang, J.; Njoki, P. N.; Luo, J.; Zhou, S.; Zhong, C.-J. *Langmuir* **2007**, *23*, 10715–10724.

(67) Link, S.; Burda, C.; Wang, Z. L.; El-Sayed, M. A. *J. Chem. Phys.* **1999**, *111*, 1255–1264.

(68) Quinten, M. *Appl. Phys. B: Laser Opt.* **2001**, *73*, 317–326.

(69) Sun, Y.; Frenkel, A. I.; Isseroff, R.; Shonbrun, C.; Forman, M.; Shin, K.; Koga, T.; White, H.; Zhang, L.; Zhu, Y.; Rafailovich, M. H.; Sokolov, J. C. *Langmuir* **2006**, *22*, 807–816.

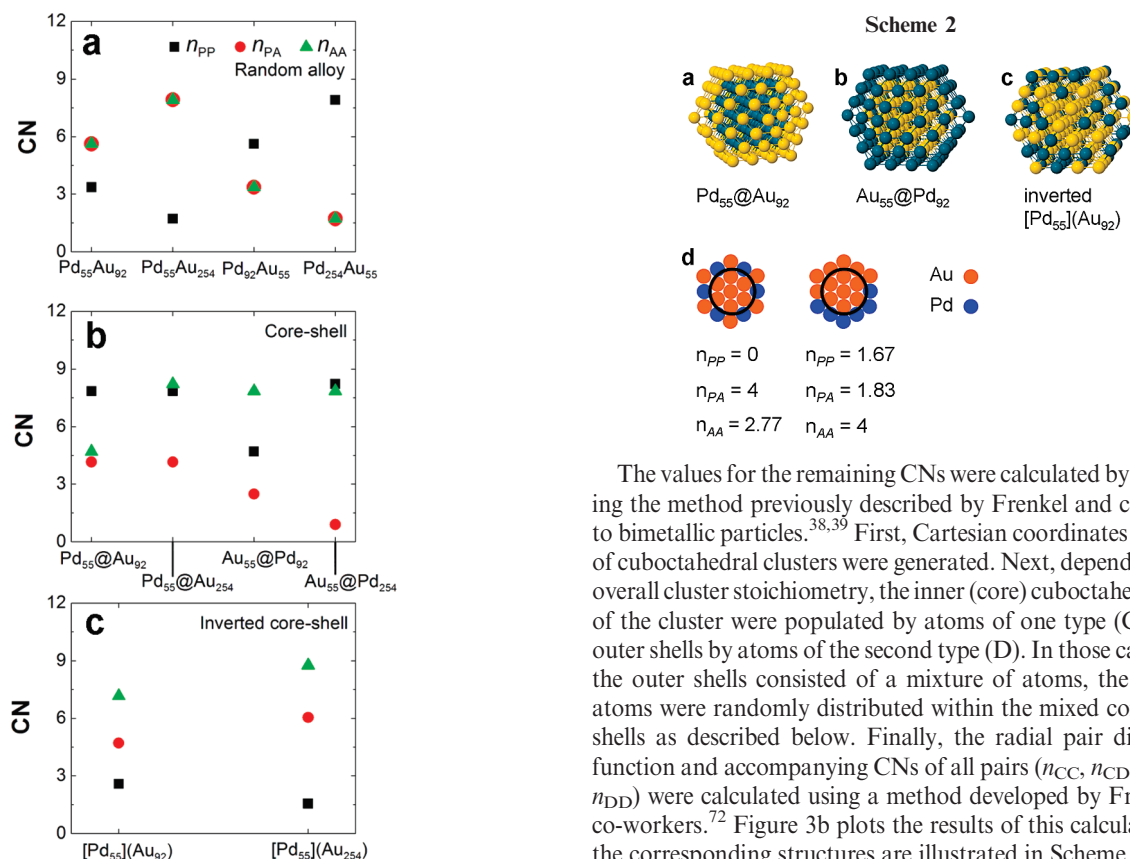


**Figure 3.** Calculated CNs for the following ideal nanoparticle configurations: (a) random alloy (theoretical), (b) core–shell, (c) inverted core–shell. Note that the CNs in (c) correspond to particles having Au cores and randomly configured PdAu shells. See text for additional information.

example, to determine the structure of bimetallic DENs, we consider six distinct CNs:  $n_{PP}$ ,  $n_{PA}$ ,  $n_{AA}$ ,  $n_{PM}$ ,  $n_{AM}$ , and  $n_{MM}$ , where  $n_{AP}$  is determined from  $n_{PA}$  and the stoichiometry of the particles. Here, A refers to Au, P to Pd, and M to any metal present (in this case, Au or Pd). The relationships between these CNs for an ideal, randomly alloyed nanoparticle have been discussed in detail elsewhere.<sup>7</sup> Briefly,  $n_{PP}$ ,  $n_{PA}$ , and  $n_{AA}$  vary linearly with the stoichiometry, and the metal CNs are all equal ( $n_{PM} = n_{AM} = n_{MM}$ ). The relevant values for the current stoichiometries were calculated and are provided in Figure 3a.

The CNs for an ideal cuboctahedral core–shell particle are more difficult to interpret, compared to monometallic particles, because there are fewer clear trends. The core metal (C) will have a  $n_{CC}$  similar to that of a smaller monometallic nanoparticle of the appropriate size. In this case, the CN for the core atoms resembles a 55-atom nanoparticle ( $n_{CC} = 7.85$ ). However, the core is surrounded by shell atoms, and therefore  $n_{CM} = 12$ , which is the bulk value. The metal CN for the shell metal (D) will be lower than 12 because the surface atoms are partially uncoordinated ( $n_{DM} < 12$ ). The value for this CN will vary with the number of shells and size of the nanoparticle. For example, the nanoparticle size will determine  $n_{MM}$ , just as it does for a monometallic nanoparticle.<sup>39,70,71</sup> Furthermore, differences between observed and calculated core and shell CNs ( $n_{CM}$  and  $n_{DM}$ ) may also arise due to interfacial disorder.

The values for the remaining CNs were calculated by generalizing the method previously described by Frenkel and co-workers to bimetallic particles.<sup>38,39</sup> First, Cartesian coordinates of a series of cuboctahedral clusters were generated. Next, depending on the overall cluster stoichiometry, the inner (core) cuboctahedral shells of the cluster were populated by atoms of one type (C) and the outer shells by atoms of the second type (D). In those cases where the outer shells consisted of a mixture of atoms, the C and D atoms were randomly distributed within the mixed composition shells as described below. Finally, the radial pair distribution function and accompanying CNs of all pairs ( $n_{CC}$ ,  $n_{CD}$ ,  $n_{DC}$ , and  $n_{DD}$ ) were calculated using a method developed by Frenkel and co-workers.<sup>72</sup> Figure 3b plots the results of this calculation, and the corresponding structures are illustrated in Scheme 2.

In addition to the theoretically calculated random alloy model and the software-based core–shell models, CNs were also calculated for one other model: an inverted Pd@Au core–shell particle. That is, a Pd@Au core–shell nanoparticle inverted to a Au@Pd structure that retains the same atomic stoichiometry. For example, the inverted structure corresponds to moving the Pd atoms in Scheme 2a to the surface of the particle and filling the new core with the Au atoms that were formerly in the shell. However, the number of metal atoms of each type remains the same: 55 Pd and 92 Au. Because the core of this 147-atom nanoparticle has space for 55 atoms, it is completely filled by Au. The remaining 37 (92 – 55) Au atoms must remain in the shell. The rest of the shell is occupied by the Pd atoms. This mixed-composition shell is assumed to be randomly occupied by Pd and Au atoms (Scheme 2c). The CNs for this inverted structure will vary depending on the shell configuration. For example, Scheme 2d shows two quite different structures that could result from inversion: segregated and alternating. In both cases the numbers of Pd and Au atoms in the shell are identical. When these types of configurations are considered, the only consistent trend is that  $n_{AM} > n_{MM} > n_{PM}$ . To simplify the analysis, therefore, the CNs reported in Figure 3c are calculated assuming a random shell. Each of these idealized models should be viewed as an illustration of different structural trends, not as actual 3D structures, due to the distribution of particle sizes and structural disorder that are present in the nanoparticles prepared by most methods.

EXAFS scans of the DENs were collected for both the Pd and Au absorption edges. As many as 12 scans were aligned in energy, using a reference foil, and then the spectra were averaged to reduce statistical noise. The data for Pd and Au edges of the same sample were fit simultaneously in *R*-space using the Artemis

(70) Jentys, A. *Phys. Chem. Chem. Phys.* **1999**, *1*, 4059–4063.

(71) Knecht, M. R.; Weir, M. G.; Myers, V. S.; Pyrz, W. D.; Ye, H.; Petkov, V.; Burrey, D. J.; Frenkel, A. I.; Crooks, R. M. *Chem. Mater.* **2008**, *20*, 5218–5228.

(72) Frenkel, A. I.; Frankel, S. C.; Liu, T. *Phys. Scr.* **2005**, *T115*, 721–723.

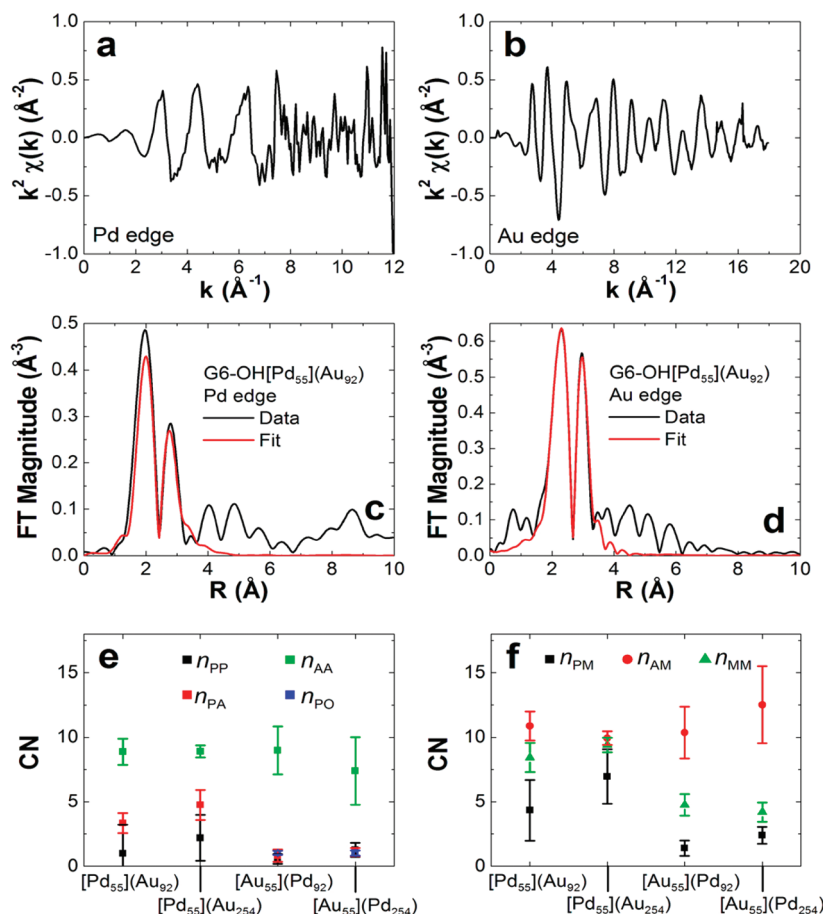


**Figure 4.** EXAFS data and corresponding fitting analyses for the DENs.  $k$ -space data are given for the (a) Pd K edge and (b) Au L<sub>3</sub> edge of G6-OH[Pd<sub>55</sub>](Au<sub>92</sub>) DENs. The corresponding Fourier transform magnitudes of the  $k^2$ -weighted data and fits are provided in frames (c) and (d), respectively. In frames (c) and (d), the data are plotted in black and the calculated fits are in red. The  $k$ -ranges from 2 to 8.3  $\text{\AA}^{-1}$  and from 2.7 to 11  $\text{\AA}^{-1}$  were used for the Pd and Au fits, respectively. The partial and metal CNs are summarized in frames (e) and (f), respectively.

program.<sup>47</sup> As in our previous paper, the number of fitted variables was reduced by constraining the bond lengths and Debye–Waller factors for Pd–Au bonds to be equivalent for each edge and by requiring the ratio of CNs of these bonds to be equal to the ratio of their bulk compositions.<sup>7</sup> That is, for Pd<sub>x</sub>Au<sub>y</sub>,  $n_{\text{PA}}/n_{\text{AP}} = y/x$ .

**EXAFS Characterization of DENs.** Parts a and b of Figure 4 provide an example of the  $k$ -space data for the G6-OH[Pd<sub>55</sub>](Au<sub>92</sub>) DENs for the Pd and Au edges, respectively. Parts c and d of Figure 4 provide the  $R$ -space data and fit results for the same material. The individual and metal CNs for all DEN configurations are plotted in parts e and f of Figure 4, respectively.

First, consider the CNs for the G6-OH[Pd<sub>55</sub>](Au<sub>92</sub>) DENs (Figures 4e). The  $n_{\text{AA}}$  is high ( $8.9 \pm 1.0$ ) when compared with  $n_{\text{PP}}$  ( $1.0 \pm 2.2$ ) and  $n_{\text{PA}}$  ( $3.3 \pm 0.8$ ). These results do not fit the alloy model where  $n_{\text{PA}} = n_{\text{AA}} = 5.6$  (Figure 3a). Likewise, they do not match the trends of the core–shell model where  $n_{\text{PP}} > n_{\text{PA}}$  and  $n_{\text{AA}}$  (Figure 3b). The model most closely matching the data is the inverted core–shell (Figure 3c). However, even this model is not a perfect fit to the data. We rationalize this as follows. First, there are variations in the possible shell configurations (Scheme 2d), and this will lead to a range of CNs. Second, we have previously shown that the structure of DENs may be somewhat amorphous and therefore different from the cuboctahedral model assumed for the calculated CNs.<sup>71,73</sup>

Next, we examine the metal CN data for the G6-OH[Pd<sub>55</sub>](Au<sub>92</sub>) DENs (Figure 4f). These data also fit the expected trends ( $n_{\text{AM}} > n_{\text{MM}} > n_{\text{PM}}$ ) for the inverted core–shell model, but not for the other two models we consider. Finally, the numerical value for the average metal CN,  $n_{\text{MM}}$ , is  $8.4 \pm 1.1$ , which is close to the CN (9.0) for an ideal 147-atom truncated cuboctahedron.

The values of the CNs for the larger G6-OH[Pd<sub>55</sub>](Au<sub>254</sub>) DENs (Figure 4e) are also only consistent with the inverted core–shell model ( $n_{\text{AA}} = 8.9 \pm 0.5$ ,  $n_{\text{PP}} = 2.2 \pm 1.8$ , and  $n_{\text{PA}} = 4.7 \pm 1.2$ ). The metal CNs (Figure 4f) fit the same trend as discussed for the G6-OH[Pd<sub>55</sub>](Au<sub>92</sub>) DENs. The average metal CN,  $n_{\text{MM}}$ , for this configuration is  $9.4 \pm 0.6$ , which is both larger than that of the smaller DENs and consistent with the value for a perfect 309 atom truncated cuboctahedron (9.6).

Next we consider the Au core materials. The G6-OH[Au<sub>55</sub>](Pd<sub>92</sub>) DENs are different from the G6-OH[Pd<sub>55</sub>](Au<sub>x</sub>) DENs in that there is a significant contribution to the EXAFS signal from Pd–O or Pd–N bonds. These types of interactions are indistinguishable, and therefore they are both modeled as Pd–O for simplicity and the CN is given as  $n_{\text{PO}}$ . This bonding is likely a combination of interactions between the Pd surface and amines or amides from the dendrimer, oxygen atoms (that is, PdO), OH<sup>−</sup>, and H<sub>2</sub>O.<sup>56</sup>

For G6-OH[Au<sub>55</sub>](Pd<sub>92</sub>),  $n_{\text{AA}}$  is relatively high ( $9.0 \pm 1.9$ ) while  $n_{\text{PA}}$  and  $n_{\text{PP}}$  are much lower ( $0.8 \pm 0.5$  and  $0.6 \pm 0.4$ ). Because EXAFS is an ensemble averaging technique, there are two models that fit these data. Either there is a Au core nanoparticle with a loose, disordered Pd shell or there is a bimodal distribution of Au

(73) Petkov, V.; Bedford, N.; Knecht, M. R.; Weir, M. G.; Crooks, R. M.; Tang, W.; Henkelman, G.; Frenkel, A. *J. Phys. Chem. C* **2008**, *112*, 8907–8911.

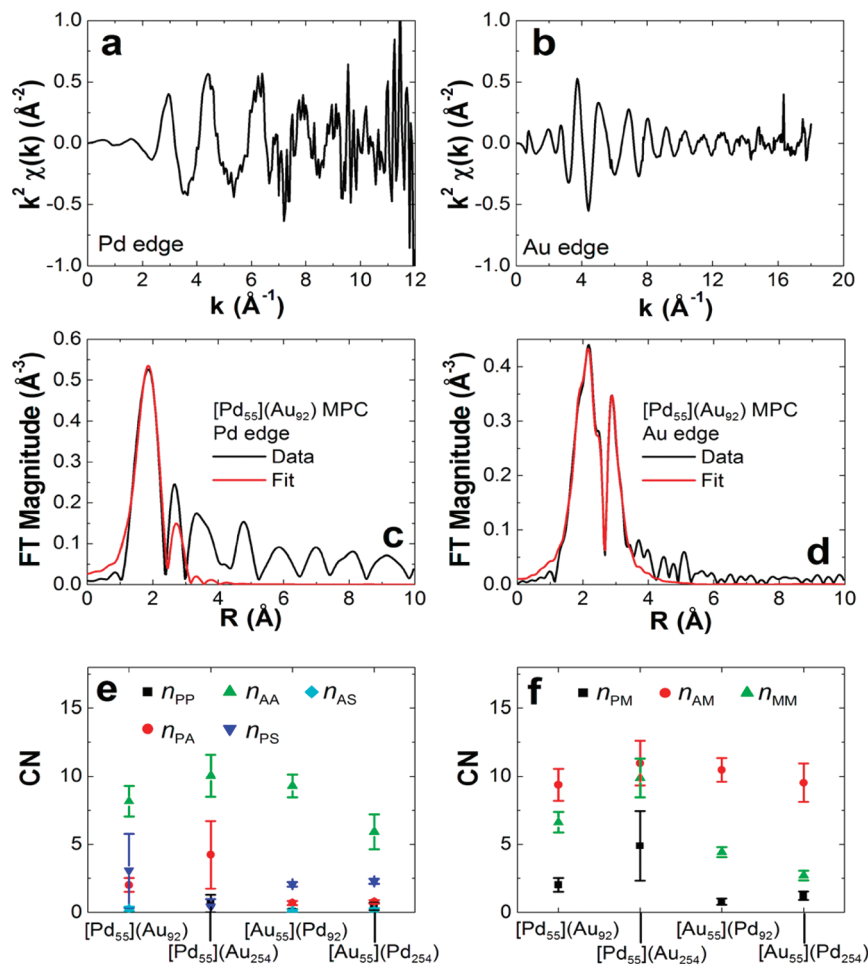


**Figure 5.** EXAFS data and corresponding fitting analyses for the MPCs.  $k$ -space data are given for the (a) Pd K edge and (b) Au L<sub>3</sub> edge of  $[\text{Pd}_{55}](\text{Au}_{92})$  MPCs. The corresponding Fourier transform magnitudes of the  $k^2$ -weighted data and fits are provided in frames (c) and (d), respectively. In frames (c) and (d), the data are plotted in black and the calculated fits are in red. The  $k$ -ranges from 3 to 10  $\text{\AA}^{-1}$  and from 3.2 to 15  $\text{\AA}^{-1}$  were used for the Pd and Au fits, respectively. The partial and metal CNs are summarized in frames (e) and (f), respectively.

nanoparticles (capped with a small amount of Pd) and a large number of small (1 to  $\sim 5$  atom), oxidized Pd clusters that are not closely associated with the Au nanoparticles. These two models can be distinguished by examining the metal CNs and comparing them with the UV–vis and TEM data. The  $n_{\text{AM}}$  ( $10.4 \pm 2.0$ ) is significantly higher than would be expected for a  $\text{Au}_{55}$  nanoparticle (7.9).<sup>39,70</sup> Therefore, the measured CN is consistent with the disordered Pd shell model but not the bimodal distribution. The minimum fraction of oxidized Pd atoms necessary to account for a  $n_{\text{PO}}$  of  $1.0 \pm 0.2$  is approximately one-quarter of the total Pd. In this case, a strong LMCT band at  $\sim 220$  nm would be expected.<sup>1,49,56</sup> Because no such band is observed, the UV–vis data are also consistent with the Au core-disordered Pd shell model. Finally, the size of the G6-OH $[\text{Au}_{55}](\text{Pd}_{92})$  particles measured by TEM is larger than previously observed for monometallic DENs containing the same total number (147) of atoms.<sup>1,49,73</sup> In the bimodal distribution model, the size should be less than or equal to that of the corresponding monometallic DENs. Note also that the average metal coordination number,  $n_{\text{MM}}$ , is significantly lower ( $4.8 \pm 0.8$ ) than that of the G6-OH- $[\text{Pd}_{55}](\text{Au}_{92})$  DENs, probably due to disorder in the Pd shell, and is lower than that of the calculated, ideal nanoparticles (9.0). We conclude that the G6-OH $[\text{Au}_{55}](\text{Pd}_{92})$  DENs have a Au@Pd structure, with the Pd shell showing disorder from bonding with O.

The analysis of the G6-OH $[\text{Au}_{55}](\text{Pd}_{254})$  DENs is similar to that of the just-discussed G6-OH $[\text{Au}_{55}](\text{Pd}_{92})$  DENs. The  $n_{\text{AA}}$

( $7.4 \pm 2.6$ ) is again higher than  $n_{\text{PA}}$  ( $1.1 \pm 0.3$ ) and  $n_{\text{PP}}$  ( $1.3 \pm 0.6$ ). The CN,  $n_{\text{AM}}$  ( $12.5 \pm 3.0$ ), is again consistent with a Au core. The same arguments as above are used with the UV–vis and TEM data, resulting in a Au@Pd structure having a partial oxidized Pd shell. The partial oxidation of the Pd shell and accompanying disorder lower the average metal CN,  $n_{\text{MM}}$ .

**EXAFS Analysis of MPCs.** The approach for analyzing extracted MPCs is very similar to that used for the DENs, but in this case the presence of metal bonds to sulfur must also be considered. An example of the  $k$ - and  $R$ -space data, the fitting analysis, and a summary of the CNs are found in Figure 5. For all of the MPCs,  $n_{\text{AA}}$  and  $n_{\text{AM}}$  remain high compared to  $n_{\text{PP}}$  and  $n_{\text{PM}}$ , indicating that the Au atoms are in the core of the material. In addition, the Au–S CN,  $n_{\text{AS}}$ , is low, indicating that few Au atoms are available for binding to S atoms. For the  $[\text{Pd}_{55}](\text{Au}_{254})$  MPCs, Au–S bonds do not contribute significantly to the fit but Pd–S bonds do. The  $n_{\text{PS}}$  ranges from  $0.4 \pm 0.5$  for  $[\text{Pd}_{55}](\text{Au}_{92})$  to  $3.1 \pm 2.7$  for  $[\text{Pd}_{55}](\text{Au}_{254})$ . Because the maximum possible Pd–S CN is 4, these results indicate that more than a surface layer of thiols is present.<sup>69,73</sup> Accordingly, we propose a model in which the outer layers of the nanoparticle are penetrated by the thiol head groups. This leads to disordering of the Pd shell and hence a lower-than-expected  $n_{\text{PP}}$  and a correspondingly higher-than-expected  $n_{\text{PS}}$ . The alternative model, which invokes the presence of a bimodal distribution of small Pd–S particles and MPCs, is not consistent with the sizes measured by TEM. Additionally, the absence of a

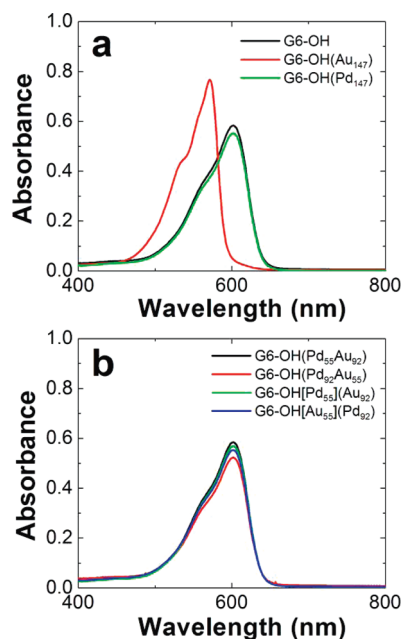


**Figure 6.** UV-vis spectra illustrating the results for the DEN-catalyzed conversion of resazurin to resorufin. (a) Spectra for G6-OH and monometallic Au and Pd DENs consisting of an average of 147 atoms. Only the Au DENs are catalytically active. (b) Spectra showing that DENs prepared by sequential reduction and co-complexation do not catalyze the resazurin-to-resorufin reaction. Spectra were measured in water, the path length of the cuvette was 0.20 cm, and the concentrations of DENs and resazurin were 40 nM and 10  $\mu$ M, respectively.

significant Au-S contribution to the EXAFS fits suggests that Au must be confined within a protective shell of Pd and hence shielded from S atoms.

**Selective Catalytic Reactions.** The reduction of resazurin to resorufin is a well-known and frequently used biological assay.<sup>74,75</sup> Both compounds have a strong, distinct absorbance in the visible range ( $\lambda_{\text{max}} = 602$  and 572 nm, respectively, at basic pH),<sup>76</sup> and there is a large difference in their fluorescence quantum yield.<sup>77</sup> As recently shown by Chen and co-workers,<sup>4</sup> this reduction is catalyzed by Au nanoparticles in the presence of amines. However, we have carried out control experiments demonstrating that this reaction is not catalyzed by Pd DENs or by the tertiary amines of the dendrimer. Accordingly, the catalytic conversion of resazurin to resorufin can be used as a probe for the composition of the surface of PdAu nanoparticles. That is, the reaction should only proceed in the presence of a Au shell. Note also that a very dilute concentration (40 nM) of Au nanoparticles is sufficient to catalyze this reaction.

Figure 6 shows the absorbance spectra in the region of interest for resazurin and resorufin. A complete UV-vis spectrum is provided in the Supporting Information (Figure S4). Part a of Figure 6 shows the effect on the conversion of resazurin in the presence of G6-OH only, and monometallic, 147-atom Au and Pd DENs. Initially, all three solutions exhibited the deep blue color typical of resazurin. There is no spectral change in the presence of the dendrimer or the Pd DENs, but upon exposure to Au DENs

the color of the solution changes to the bright pink color of resorufin. This change is observed in part a of Figure 6 as a shift in  $\lambda_{\text{max}}$  from 602 to 571 nm and in the shape of the spectrum. Additional control experiments were carried out for conditions similar to those used to prepare the monometallic and bimetallic DENs, but with no metals added. These data are not shown because there was no detectable conversion of resazurin to resorufin.

Part b of Figure 6 presents spectra for the sequentially reduced DENs, G6-OH[Pd<sub>55</sub>](Au<sub>92</sub>) and G6-OH[Au<sub>55</sub>](Pd<sub>92</sub>), and those prepared by co-complexation with the same stoichiometry: G6-OH(Pd<sub>55</sub>Au<sub>92</sub>) and G6-OH(Pd<sub>92</sub>Au<sub>55</sub>). None of these bimetallic nanoparticles catalyze the conversion of resazurin to resorufin. The catalysis results for DENs prepared by sequential reduction are in agreement with the EXAFS analysis, which showed that the Au atoms are predominantly located within the interior of the particles rather than on the surface. It is somewhat surprising that the same result is obtained for the DENs prepared by co-complexation because our previous EXAFS results showed that some Au atoms are on the surface of these nanoparticles.<sup>7</sup> This suggests that this catalytic reaction requires particular configurations of Au atoms on the particle surface. For example, isolated Au atoms may be less catalytically active compared to, for example, Au atoms on the surface of G6-OH(Au<sub>55</sub>) monometallic DENs. Consistent with this view, Goodman and co-workers have recently observed that contiguous Pd atoms on a Au surface promote CO oxidation.<sup>78</sup> A similar argument can be made for the lack of catalytic activity of G6-OH[Pd<sub>55</sub>](Au<sub>254</sub>) DENs, which must have some Au on the surface because of the large Au:Pd ratio.

## Summary and Conclusions

We have prepared PdAu DENs via the two sequential reduction methods shown in Scheme 1. When Au is reduced onto 55-atom, preformed Pd DEN cores, the data analysis leads to a model consistent with inversion of the two metals. That is, Au migrates into the core and Pd resides on the surface. However, when Pd is reduced onto a 55-atom Au core, the expected Au@Pd structure results. However, in this latter case, the EXAFS analysis suggests partial oxidation of the relatively thick Pd shell. The absence of such oxidation in the inverted structures is likely a consequence of the relatively low surface concentration of Pd in these materials and an apparent stabilization of surface Pd by Au. When the DENs are extracted from their protective dendrimer stabilizers by alkylthiols, the resulting MPCs retain the original Au@Pd structures. However, the presence of the thiol groups leads to some subtle structural changes in the Pd shells that are revealed by EXAFS.

Results relating to the catalytic conversion of resazurin to resorufin by DENs are especially interesting. We find that monometallic G6-OH(Au<sub>147</sub>) and G6-OH(Au<sub>55</sub>) DENs efficiently catalyze this reaction. In contrast, none of the PdAu DENs prepared by sequential reduction are active. This result is certainly consistent with the presence of a Au core surrounded by a protective Pd shell, as suggested by EXAFS. Interestingly, however, the G6-OH[Pd<sub>55</sub>](Au<sub>254</sub>) DENs, which must have a substantial number of Au atoms on their surfaces (due to high Au: Pd ratio) after inversion, are still not catalytically active. This suggests that the conversion of resazurin to resorufin requires particular spatial relationships between Au atoms that are not present on sequentially reduced PdAu DENs. Indeed, even PdAu

(74) Karakashev, D.; Galabova, D.; Simeonov, I. *World J. Microbiol. Biotechnol.* **2003**, *19*, 233–238.

(75) Chapin, K. C.; Lauderdale, T.-L. *Manual of Clinical Microbiology*; Murray, P. R., Ed.; ASM Press: Washington, DC, 2007.

(76) Bueno, C.; Villegas, M. L.; Bertolotti, S. G.; Previtali, C. M.; Neumann, M. G.; Encinas, M. V. *Photochem. Photobiol.* **2002**, *76*, 385–390.

(77) Guilbault, G. G.; Kramer, D. N. *Anal. Chem.* **1965**, *37*, 1219–1221.

(78) Gao, F.; Wang, Y.; Goodman, D. W. *J. Am. Chem. Soc.* **2009**, *131*, 5734–5735.

DENs prepared by co-complexation, which have quasi-random alloy structures, are not catalytically active for this reaction.

The key conclusion from this work is that correlation of structure to catalytic function for very small, bimetallic nanoparticles requires detailed information about atomic configuration. Underscoring this point is our finding that the synthesis of bimetallic PdAu nanoparticles may yield unanticipated structures, such as the inverted Au@Pd DENs reported here. Clearly the structure of nanoparticles in the  $< 2$  nm size range may be controlled by factors that are, at present, not understood. Unfortunately, unambiguous structure determination for particles in this size range remains a major analytical challenge.

**Acknowledgment.** M.G.W., M.R.K., and R.M.C. gratefully acknowledge support from the Chemical Sciences, Geosciences, and Biosciences Division, Office of Basic Energy Sciences, Office of

Science, U.S. Department of Energy (Contract DE-FG02-05ER15683), and the National Science Foundation (Grant 0847957) for support of this research. We also thank Sue V. Myers for assistance with the resazurin experiments. A.I.F. acknowledges support of the Department of Energy Grant DE-FG02-03ER15476. Use of the NSLS was supported by the U.S. Department of Energy, Office of Science, Office of Basic Energy Sciences, under Contract DE-AC02-98CH10886. Beamline X18B at the NSLS is supported in part by the Synchrotron Catalysis Consortium, U.S. Department of Energy, Grant DE-FG02-05ER15688.

**Supporting Information Available:** TEM micrographs and particle-size distributions for monometallic and bimetallic DENs and bimetallic MPCs; full UV-vis spectra corresponding to the resazurin experiment. This material is available free of charge via the Internet at <http://pubs.acs.org>.